Efficient Patient-Specific Simulations of Ventricular Tachycardia Based on Computed Tomography-Defined Wall Thickness Heterogeneity

Nicolas Cedilnik, Mihaela Pop, Josselin Duchateau, Frédéric Sacher, Pierre Jaïs, Hubert Cochet, Maxime Sermesant

JACC: CLINICAL ELECTROPHYSIOLOGY VOL. ■, NO. ■, 2023

ORIGINAL RESEARCH PAPER

Efficient Patient-Specific Simulations of Ventricular Tachycardia Based on Computed Tomography-Defined Wall Thickness Heterogeneity

Nicolas Cedilnik, PhD,[a,b] Mihaela Pop, PhD,[a] Josselin Duchateau, MD, PhD,[b,c] Frédéric Sacher, MD, PhD,[b,c] Pierre Jaïs, MD, PhD,[b,c] Hubert Cochet, MD, PhD,[b,d] Maxime Sermesant, PhD[a,b]

ABSTRACT

BACKGROUND Electrophysiological mapping of ventricular tachycardia (VT) is tedious and poorly reproducible. Substrate analysis on imaging cannot explicitly display VT circuits.

OBJECTIVES This study sought to introduce a computed tomography-based model personalization approach, allowing for the simulation of postinfarction VT in a clinically compatible time frame.

METHODS In 10 patients (age 65 ± 11 years, 9 male) referred for post-VT ablation, computed tomography-derived wall thickness maps were registered to 25 electroanatomical maps (sinus rhythm, paced, and VT). The relationship between wall thickness and electrophysiological characteristics (activation-recovery interval) was analyzed. Wall thickness was then employed to parameterize a fast and tractable organ-scale wave propagation model. Pacing protocols were simulated from multiple sites to test VT induction in silico. In silico VTs were compared to VT circuits mapped clinically.

RESULTS Clinically, 6 different VTs could be induced with detailed maps in 9 patients. The proposed model allowed for fast simulation (median: 6 min/pacing site). Simulations of steady pacing (600 milliseconds) from 100 different sites/patient never triggered any arrhythmia. Applying S1-S2 or S1-S2-S3 induction schemes allowed for the induction of in silico VTs in the 9 of 10 patients who were clinically inducible. The patient who was not inducible clinically was also noninducible in silico. A total of 42 different VTs were simulated (4.2 ± 2 per patient). Six in silico VTs matched a VT circuit mapped clinically.

CONCLUSIONS The proposed framework allows for personalized simulations in a matter of hours. In 6 of 9 patients, simulations show re-entrant patterns matching intracardiac recordings. (J Am Coll Cardiol EP 2023;■:■–■)

From the [a]Université Côte d'Azur, Epione, Inria, Sophia-Antipolis, France; [b]Institut Hospitalo-Universitaire Liryc, Bordeaux, France; [c]Cardiac Pacing and Electrophysiology Department, Bordeaux University Hospital, Bordeaux, France; and the [d]Radiology Department, Bordeaux University Hospital, Bordeaux, France.
The authors attest they are in compliance with human studies committees and animal welfare regulations of the authors' institutions and Food and Drug Administration guidelines, including patient consent where appropriate. For more information, visit the Author Center.

Manuscript received October 31, 2022; revised manuscript received July 20, 2023, accepted August 2, 2023.

ISSN 2405-500X https://doi.org/10.1016/j.jacep.2023.08.008

ABBREVIATIONS AND ACRONYMS

3D = 3-dimensional

APD = action potential duration

ARI = activation-recovery interval

CL = cycle length

CMR = cardiac magnetic resonance

CT = computed tomography

DI = diastolic interval

EAM = electroanatomical map(ping)

ECG = electrocardiograph

EP = electrophysiology

ICD = implantable cardioverter-defibrillator

LV = left ventricle

RV = right ventricle

UEG = unipolar electrogram

VT = ventricular tachycardia

WT = wall thickness

Scar-related ventricular tachycardia (VT), most often occurring on postinfarction scars, can degenerate into lethal ventricular fibrillation and is a salient cause of sudden cardiac death in the world.[1] The identification of scar-related VT circuits is complicated by the invasive nature of the catheter-based diagnosis procedure performed in the clinical electrophysiology (EP) laboratory. This procedure requires not only to precisely localize the critical isthmus of VTs via a tedious mapping of intracardiac electrical signals, but also to induce VTs by employing rapid pacing in programmed stimulation protocols.[2] Unfortunately, catheter-based electrical mapping often fails to detect concealed VT isthmuses within scar or at its periphery. In addition, in many patients the VT is inaccessible to mapping because the VT is noninducible, nonsustained, or not hemodynamically tolerated. In fact, the inducibility test is often not performed when patients are already hemodynamically unstable in sinus rhythm.[3] Thus, alternative solutions are clearly needed to improve VT diagnosis in a less-invasive manner and to more effectively guide ablative therapies to eliminate VT.

In the past decade, computational modeling and simulation approaches have emerged as a noninvasive alternative to virtually explore VT inducibility using clinical or preclinical data[4,5] and to plan the ablation procedure.[6] Nevertheless, to enable biophysical simulations that are both accurate and clinically translatable, these virtual heart models need explicit parameterization from detailed and patient-specific anatomical, structural, and electrical data. In particular, the accurate simulation of scar-related VT inducibility depends on our ability to integrate into these 3-dimensional (3D) heart models the precise geometry of the re-entry circuit,[7] as well as the spectrum of EP characteristics of critical channels such as action potential duration (APD) and conduction velocity. Typically, the location, shape, and heterogeneity of infarcted areas (ie, unexcitable dense scars and critical channels) are clinically identified by means of imaging[8] with contrast-enhanced cardiac magnetic resonance (CMR)[9,10] or computed tomography (CT) imaging.[11] Unlike CMR, multidetector CT scan advantageously facilitates image acquisition at sub-millimetric resolution while circumventing severe implantable cardioverter-defibrillator (ICD)-related CMR artifacts. Therefore, we recently demonstrated that wall thickness (WT) mapping from CT can identify channels of relatively preserved thickness within severely thinned scar that colocalize with VT isthmuses identified by electroanatomical mapping (EAM).[11,12] With respect to EP characteristics, conventional catheters used for EAM are technologically limited and cannot directly capture the full repolarization phase; therefore, APD cannot be directly measured. However, using the QRS interval and T waves on intracardiac electrograms, one can estimate a surrogate of APD, an activation-recovery interval (ARI).[13,14] This type of measurement could thus be used to derive the parameters associated with cardiac depolarization-repolarization phases in computational models.

The aim of this work was to introduce a fast and clinically tractable computational approach for patient-specific simulation of postinfarction VT. First, this work investigates the relation between ARI and CT-based geometrical features of chronic postinfarction scars and then assesses whether integrating this knowledge into personalized heart models leads to clinically relevant simulations of VT.

METHODS

Image acquisition and segmentation methods are detailed in the Supplemental Appendix.

STUDY POPULATION. A cohort of 10 patients was retrospectively recruited from the VT ablation program at Bordeaux University Hospital. The only inclusion criteria were a history of catheter ablation for postinfarction (6 posterior, 3 anterior, and 1 apicoseptal) VT with available preprocedural CT scan and multiple high-density EAMs acquired with the Rhythmia System (Boston Scientific). The imaging and EP data were pseudonymized and then transferred for processing at the Institut Hospitalo-Universitaire Liryc (Bordeaux, France) and Inria Sophia Antipolis (Sophia Antipolis). At the time of their ablation procedures, all patients had provided informed consent for the secondary use of their clinical data in this research project, which conformed to the French national law (MR-004) and recommendations from the Commission Nationale de l'Informatique et des Libertés. The study was approved by the Comité de Protection des Personnes (ethics committee) of Dijon (EST 1, CH la Chartreuse).

EAM AND ARI ANALYSIS AS A FUNCTION OF WT. All patients had undergone an EP mapping procedure using a 3D EAM system (Rhythmia, Boston Scientific) and a multielectrode basket catheter dedicated to high-density mapping (Orion, Boston Scientific). During the interventional EP procedure, several EAMs were recorded in each patient, including in sinus

rhythm as well as during right ventricular (RV) and left ventricular (LV) pacing and macro-re-entrant VT mapping. Administration of antiarrhythmic drugs was suspended 5 half-lives before ablation, except for amiodarone because of its longer half-life.

The EAMs were primarily acquired for building activation maps of local depolarization time. Additionally, in 26 EAMs across a subset of 9 patients, the electrogram acquisition window was sufficiently wide (600-1,000 milliseconds) to allow the detection of repolarization waves. The number of recorded electrograms per patient being very large (20,000 per patient on average; Supplemental Table 1), we developed an in-house algorithm to detect repolarization waves and accurately estimate the ARIs. The algorithm output was the ARI, which was further used as a surrogate of APD measurement. Refer to the Supplemental Appendix for details about EAM/CT registration and ARI detection.

Next, we investigated the behavior of ARI as a function of cycle length (CL) at different levels of WT, and this relationship was later used to parameterize the computational model. We started by constructing the well-known restitution curve using the data recorded in all patients: in sinus rhythm, during RV/LV pacing at several frequencies, as well as during the induced VT episodes. We fitted the measured ARI values as a function of diastolic intervals (DIs) in response to different pacing frequencies, where DI was obtained by subtracting ARI from CL (ie, DI = CL − ARI). We further estimated the relationship between ARIs and CT-derived WT and grouped the ARI values by different WT bins using 1-mm incremental steps. We thus obtained ARI values for each WT bin (eg, WT <1 mm, 2 mm, 3 mm).

CT-BASED 3D MODEL PARAMETERIZATION AND SIMULATIONS. For the simulation of cardiac transmembrane potential dynamics at cellular level, we implemented a modified version[15] of the 2-variable Mitchell-Schaeffer model,[16] by incorporating an excitability parameter that controls the amount of external current required to trigger the action potential propagation. Furthermore, at tissue-level, our model was coupled with a diffusion term and solved using a lattice-Boltzmann scheme as in Rapaka et al.[17] This versatile method leverages on the power of consumer grade's general purpose of parallel graphics processing units, which are specifically designed for large-scale data sets. This allowed for computing simulations results in a matter of minutes, which is clinically tractable.

The propagation speed of the depolarization wave was parameterized in relation to the CT-defined WT, as in our previous study (**Figure 1**).[18] Likewise, to account for tissue anisotropy, for our models we generated synthetic fibers using a rule-based method.[19] The conduction velocity was set to be virtually null in zones of severe thinning, whereas in areas with WT >5 mm it reached a plateau value of 0.8 m/s in the direction parallel to the fiber. Our previous work used a slower velocity (0.6 m/s) for the plateau because of the isotropic propagation. Here, the propagation speed was set to be 2.5× slower in the direction transverse to myocardial fibers.

The excitability parameter in different LV zones followed a similar pattern, being virtually null in the zones of severe thinning and having a plateau value for WT >5 mm, with a continuum of excitability values in between. To consider the physiological thinning of the LV base and apex, the excitability was increased in these areas. Tuning APD in the model was done according to the relationship between APD and WT obtained in the first part of the study. Briefly, APDs were set to be longer than in the normal myocardium in the zones of severe thinning (WT <3 mm) compared to other zones, noting that this APD prolongation was more significant as the thinning became more severe. Finally, we selected the same parameters for the RV wall tissue as for the healthy LV wall.

PACING SITES AND VIRTUAL PACING PROTOCOL. Personalized 3D image-based biventricular models were built from individual CT scans of the 10 patients included in this study. Then 100 pacing sites were automatically determined for each LV anatomy average Euclidian distance between 2 neighboring sites: 9 mm (see details in the Supplemental Table 2).

The **Central Illustration** illustrates the general flowchart of the in silico VT stimulation protocol performed in sequential order from the 100 virtual sites (1 at a time), as indicated by the green arrows. Furthermore, from each of these 100 automatically chosen sites, we conducted several in silico pacing protocols, replicating the typical VT inducibility tests done in the clinical catheterization lab. Explicitly, we first applied a train of pacing stimuli S1 at 600-millisecond intervals, followed by either an S2 extra-stimulus or a combination of S2-S3 extra-stimuli with decremental coupling intervals until the refractory period was reached (loss of capture).

Whenever needed, the stimulation protocol was repeated using a faster pacing rate with S1 = 400 milliseconds. A combination of pacing site and sequence of extra-stimuli (eg, S1-S2-S3) was considered "inducible" when a VT event lasted for at least

FIGURE 1 From CT to EP Parameters

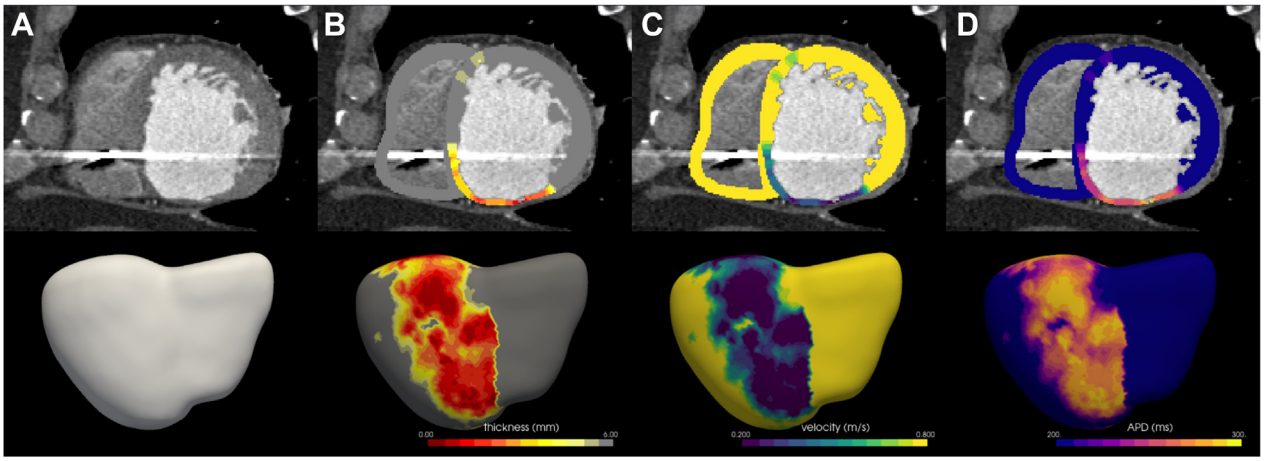

(A) High-resolution computed tomography (CT) image in short-axis **(top)** and 3-dimensional CT-derived heart segmentation **(bottom).** Derived maps: **(B)** wall thickness map (mm); **(C)** conduction velocity map (m/s); and **(D)** action potential duration (ms) at 100 beats/min.

CENTRAL ILLUSTRATION Flowchart of 3-Dimensional Computed Tomography-Based Biventricular Model Construction

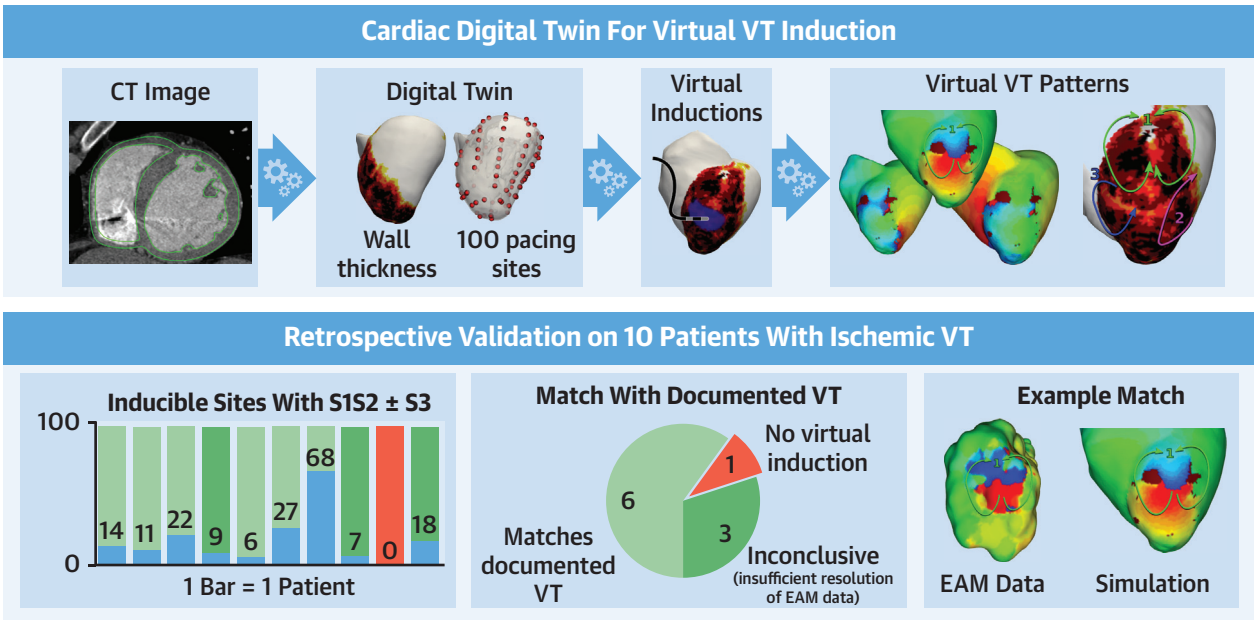

Cedilnik N, et al. J Am Coll Cardiol EP. 2023;■(■):■-■.

In silico testing of stimulation protocols from 100 pacing sites to study ventricular tachycardia (VT) patterns. CT = computed tomography; EAM = electroanatomical mapping.

FIGURE 2 APD/Wall Thinning Relationship

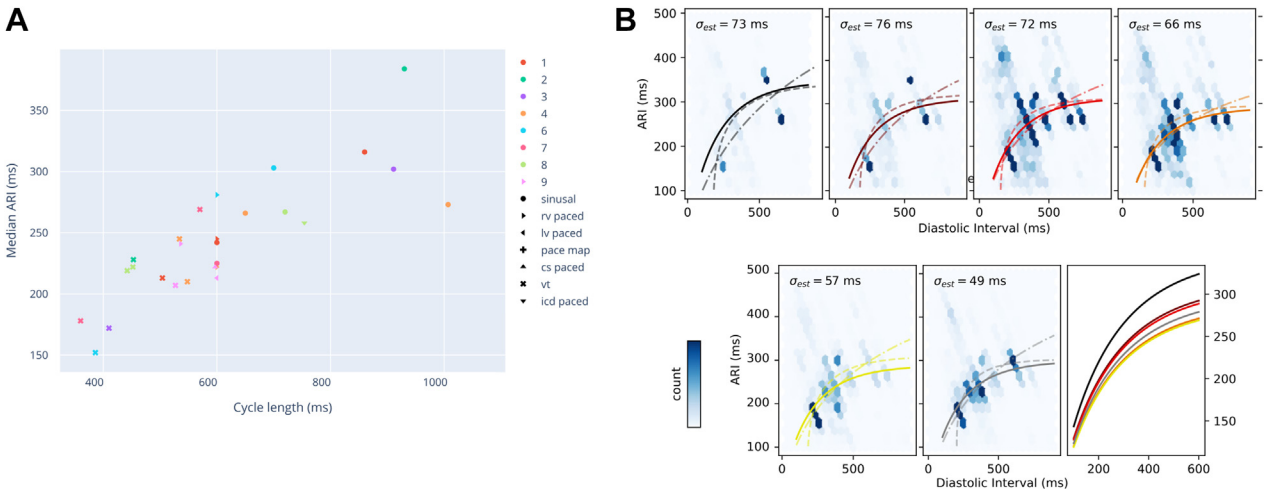

(A) Restitution curve activation-recovery interval (ARI) = f (cycle length) plotted at different pacing frequencies recorded from selected patients; **(B)** estimated correlations between ARI and computed tomography-derived wall thickness, at different levels (1-mm incremental step). APD = action potential duration; CS = coronary sinus; ICD = implantable cardioverter-defibrillator; LV = left ventricular; RV = right ventricular; VT = ventricular tachycardia.

10 seconds after the last applied stimulus. In this case, the in silico VT event was recorded, the in silico study was stopped for this site, and the protocol was restarted for the next pacing site. Lastly, similar VT patterns were automatically grouped using a clustering algorithm (see the Supplemental Figure 1).

RESULTS

POPULATION AND CLINICAL DATA. Ten patients were included (age 65 ±11 years; 9 male; mean LV ejection fraction: 34% ± 5%). All had a prior history of myocardial infarction and a documented sustained VT episode treated with either ICD shock or antitachycardia pacing. All preoperative CT scans were considered of appropriate quality, and all showed postinfarction scars visible as areas of LV wall thinning. The scar location was anterior in 3 patients, inferior in 1 patient, and posterior in 6 patients. High-density mapping was successfully performed in all patients. VT could be induced in 9 of 10 patients, but 1 patient remained noninducible despite the application of a complete VT stimulation protocol. VT circuit could be mapped in 6 patients. Overall, the mapping material available in the studied population comprised 27 maps, including 6 maps during VT, 8 maps in sinus rhythm, 9 maps during LV pacing, and 4 maps during RV pacing (average number of points per map: 11,112).

CORRELATION BETWEEN ARI AND CT-DEFINED WT. Image segmentation and registration to EAM data were successfully achieved in all patients. Figure 2A presents a scatterplot of the median ARI vs CL, using ARIs from 191,097 unipolar electrograms (UEGs) recorded at different frequencies during sinus rhythm, pacing of RV, pacing of LV, pacing from coronary sinus, catheter-induced VT episodes, and pacing done by the ICD device. These UEGs were selected from 26 different EAMs, and median per-map ARIs from 150 milliseconds to 370 milliseconds.

Figure 2B shows results from fitting the ARI as a function of DI (ie, at different heart rates), corresponding to different CT-derived WT levels (1-mm incremental steps). The dense point clouds were obtained by grouping UEGs across all EAMs by levels of WT following the registration between EAMs and CT thickness maps. Notably, by fitting ARI restitution curves, we observed a lengthening of ARI in relation to the severity of the thinning in zones of dense scar where WT <3 mm. However, this ARI lengthening was not observed for zones of moderate LV thinning (3-5 mm), where a slight shortening of APD was instead observed.

DESCRIPTION OF A SIMULATED VT INDUCTION PROTOCOL. Figure 3 presents snapshots of the simulated transmembrane potential from 1 personalized patient case. The time frames were obtained following the application of a clinical S1-S2-S3

FIGURE 3 Virtual VT Induction Protocol Using S1-S2-S3 Stimuli

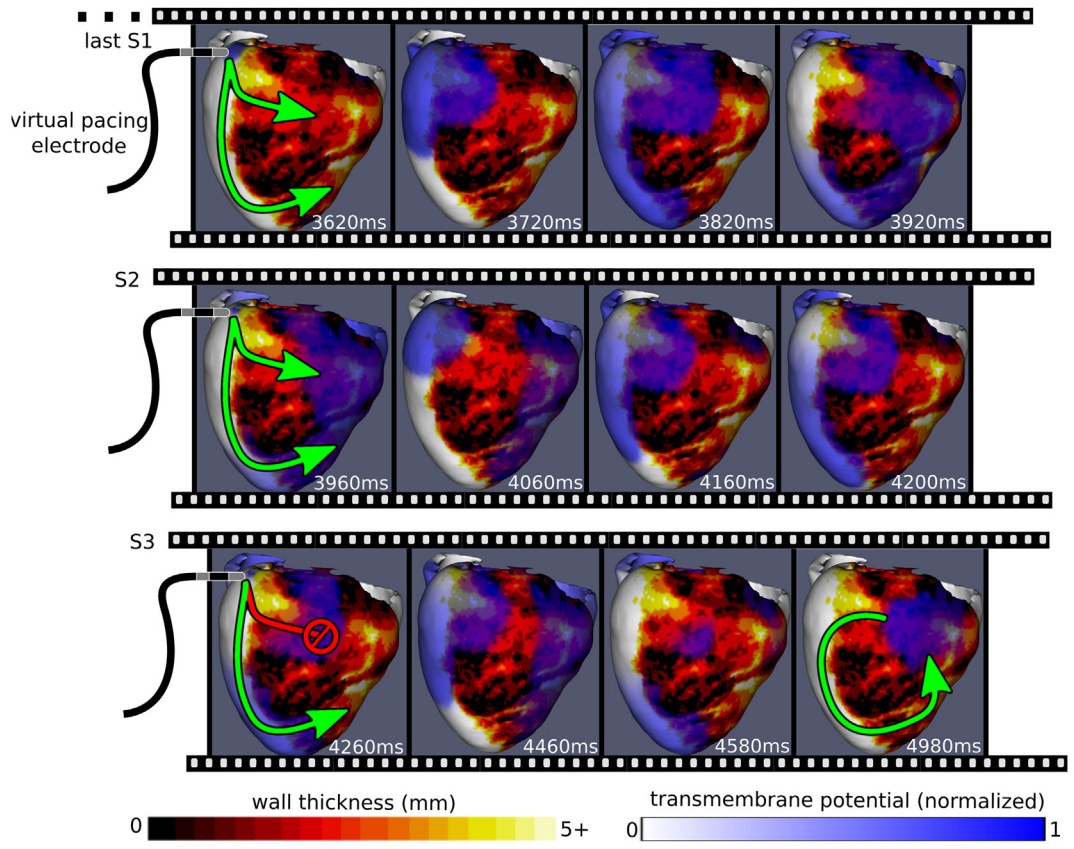

Successful virtual ventricular tachycardia (VT) induction protocol in one patient, using a typical combination of S1-S2-S3 train of stimuli. The sequential time frames show the simulated transmembrane potential (shades of **blue**, normalized values) overlayed onto the myocardial wall thickness map; the associated wave front propagating in the direction indicated by the **green arrows.** The **red arrow** indicates a path of conduction block where the tissue is not yet fully repolarized and cannot propagate the transmembrane potential.

protocol to induce VT. The stimuli were applied at the tip of the virtual pacing electrode as indicated in the figure (1 of the 100 automatically selected sites). Specifically, in the sequence of temporal frames, the solution of transmembrane potential is shown after a train of 7 S1 pacing stimuli applied at 600-millisecond intervals, which was further followed by premature S2 and S3 stimuli. In this case, neither a rapid pacing via 7 S1 stimuli, nor a train of 7 S1 stimuli followed by a S2 stimulus were able to induce VT waves, because these protocols resulted in propagating waves that annihilated each other. However, the 7 × S1 + S2 combination enabled the wave generated by S3 extrastimulus to reach a vulnerable window of the refractory period in the VT substrate (ie, critical channels of slow conduction and altered APD), which triggered a self-sustained VT wave that rotated around unexcitable scars.

One full in silico VT study (ie, simulation of the pacing protocol followed by the propagation of resulting VT waves through the critical channels and around the scar) took between 30 seconds and 19 minutes per pacing site (median: 6 ± 2 minutes) on a consumer-grade hardware, depending on how easily a self-sustained arrhythmia was induced.

IN SILICO INDUCIBILITY AND CHARACTERISTICS OF SIMULATED VTs. S1 pacing at a slow rate (600 milliseconds) did not induce any VT in any of the 10 patients, regardless of the pacing site. On the contrary, the application of VT-induction protocols using combined S1-S2 or S1-S2-S3 stimuli triggered at least 1

TABLE 1 Summary of Inducibility per Case

Patient	Induction by Slow Pacing (S1)	Induction With Dedicated Protocol (S1-S2 or S1-S2-S3)	Matching of in Silico VT With Clinical VT Pattern	Inducible Sites (Inducibility Rate) (n)	Distinct VT Patterns in Simulations (After Clustering) (n)	Simulated VTCL (ms)	Clinically Recorded VTCL (ms)
1	✗	✔	✔	14	7	560	507
2	✗	✔	✔ (mirror pattern)	11	3	440	456
3	✗	✔	✔	22	4	560	410
4	✗	✔	✗	9	5	N/A	560
5	✗	✔	✔	6	3	320	260
6	✗	✔	✔	27	2	420	270
7	✗	✔	✔	68	10	580	446
8	✗	✔	✗	7	5	N/A	N/A
9	✗	✗	✗	0	0	N/A	N/A
10	✗	✔	✗	18	3	N/A	N/A

N/A = not applicable.

self-sustained VT in 9 of 10 patients, whereas in 1 case, VT remained not inducible. Interestingly, all 9 patients who were clinically inducible during the ablation procedure were inducible in silico, but in the remaining patient, VT was not inducible during the clinical VT study or in the simulations.

Notably, some models appeared to be more arrhythmogenic than others, the number of pacing sites from which VT could be induced being highly variable, ranging from 6 to 68 sites in inducible patients (median: 12.5 sites). In most cases we were able to virtually induce VT patterns with similar electrocardiograph (ECG) waves using different combinations of pacing sites and S1-S2 or S1-S2-S3 protocols. VTs could be induced from pacing sites close to or distant from the scar. Overall, a mean of 4.2 ± 2.4 distinct VT morphologies per patient could be identified from simulation results. These simulated VTs had a median CL of approximately 490 milliseconds (minimum: 310 milliseconds, maximum: 625 milliseconds, median: 490 milliseconds, mean: 481 ± 82 milliseconds).

All results related to the VT inducibility tests are indicated in **Table 1**, where we included the number of different output patterns per patient after the clustering of distinctive simulated VT patterns, as well as the associated VTCL for inducible cases in simulations vs the clinical recordings.

COMPARISON BETWEEN CLINICAL AND SIMULATED VTs. The simulated VTs matched the VT circuits mapped clinically in 6 of 9 inducible patients (average difference in CLs: 77 milliseconds, range 15-150 milliseconds). Among these, a mirror VT pattern matching the VT mapped clinically was observed in 2 patients. In the 3 remaining patients none of the simulated VT patterns matched with the clinically mapped VTs, despite their localization in myocardial wall thinning. Of note, 2 clinically induced VTs in 2 patients could not be compared to simulated VTs because the spatial resolution of the EAM was deemed too low to provide a conclusive judgment.

Figures 4 to 7 show representative examples of simulation results selected from the patients with inducible VT, along with corresponding activation maps acquired clinically. For a more comprehensive look at the simulation results, these can be visualized in the Supplemental Appendix, where all output simulations were saved as activation maps and as variations of transmembrane potential over time, including during the VT-induction phase.

DISCUSSION

Predictive modeling approaches have become ubiquitous in EP applications pertaining to noninvasive arrhythmia diagnosis and treatment planning. Especially, simulations using image-based heart models can help us estimate the action potential wave propagation, identify patients with chronic infarct at risk of dangerous arrhythmia, and optimize guidance of interventional ablative therapies.[6,7,10] In this in silico study, we effectively implemented a novel methodology to parameterize APD in the Mitchell-Schaeffer computational model and to forecast possible patterns of induced VT from many possible stimulation sites, validating the model feasibility in a pilot study of 10 patients with chronic scars in which the clinical outcomes of VT inducibility tests were available. Moreover, in this work we expanded our previous method of building 3D CT-based models,[18] by integrating into the model key features of ARI (ie, clinical surrogate of APD) as a function of different depths of WT. Overall, our personalized models coupled with

FIGURE 4 **Simulated vs Recorded VT Patterns (Patient 6)**

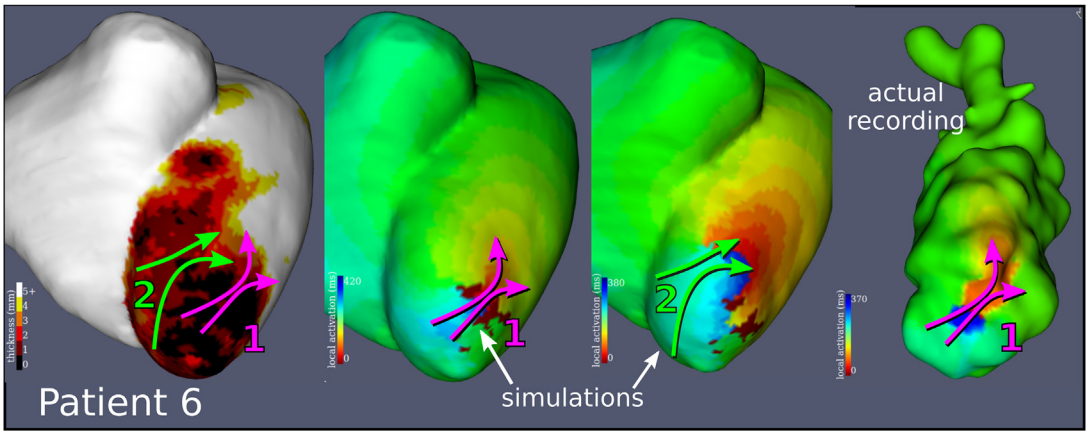

In this case, 2 potential isthmuses (critical channels) and associated macro-re-entrant ventricular tachycardia (VT) patterns were identified in simulations: 1 **(magenta arrow)** and 2 **(green arrow).** In the activation maps during VT obtained from both simulations and electroanatomical mapping recordings, **red** corresponds to early depolarization times (ie, indicating the point where the VT wave exits the isthmus and depolarizes the distal healthy myocardium) and **blue** corresponds to areas depolarized latest (ie, the entrance of VT wave in the isthmus channel, where the tissue is repolarized).

advanced numerical methods were able to successfully predict VT inducibility in all 9 patients with VT, as well as noninducibility in the only patient who was noninducible in this pilot study. Notably, the resulting simulated 12-lead ECG waves during VT were successfully clustered using a standard hierarchical similarity algorithm, whereas our custom implementation of a combined graphics processing unit-meshless approach resulted in clinically attractive times (ie, approximately 1 minute per stimulation site, 1-2 hours per case).

CONSTRUCTION OF STRUCTURAL 3D CT-BASED HEART MODELS. First of all, in this work we constructed anatomical models from 3D CT images whose spatial resolution is clearly superior to the one currently achievable by clinical CMR scans, allowing us to build detailed 3D heart models. Noteworthy,

FIGURE 5 **Simulated vs Recorded VT Patterns (Patient 1)**

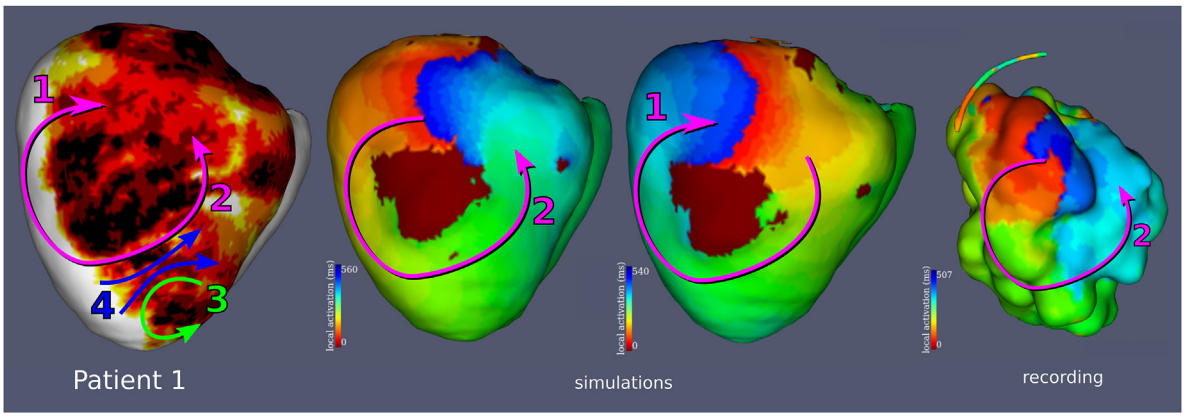

We found 4 potential paths indicated by **magenta, blue, and green arrows (left).** The 2 mirrored activation patterns of the ventricular tachycardia (VT) wave rotating around the scar are shown (**center and right**, respectively).

FIGURE 6 **Simulated vs Recorded VT Patterns (Patient 3)**

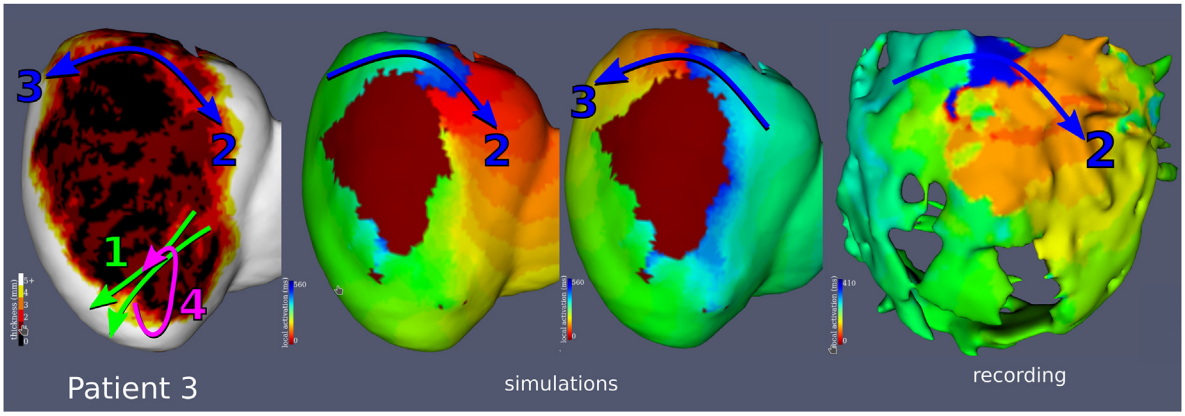

One simulated path (indicated by **arrow 2**) matched the epicardial electroanatomical map, whereas another path **(arrow 3)** was its mirror reflection, and the ventricular tachycardia (VT) wave rotated around the scar in the opposite direction.

FIGURE 7 **Simulated vs Recorded VT Patterns (Patients 5 and 7)**

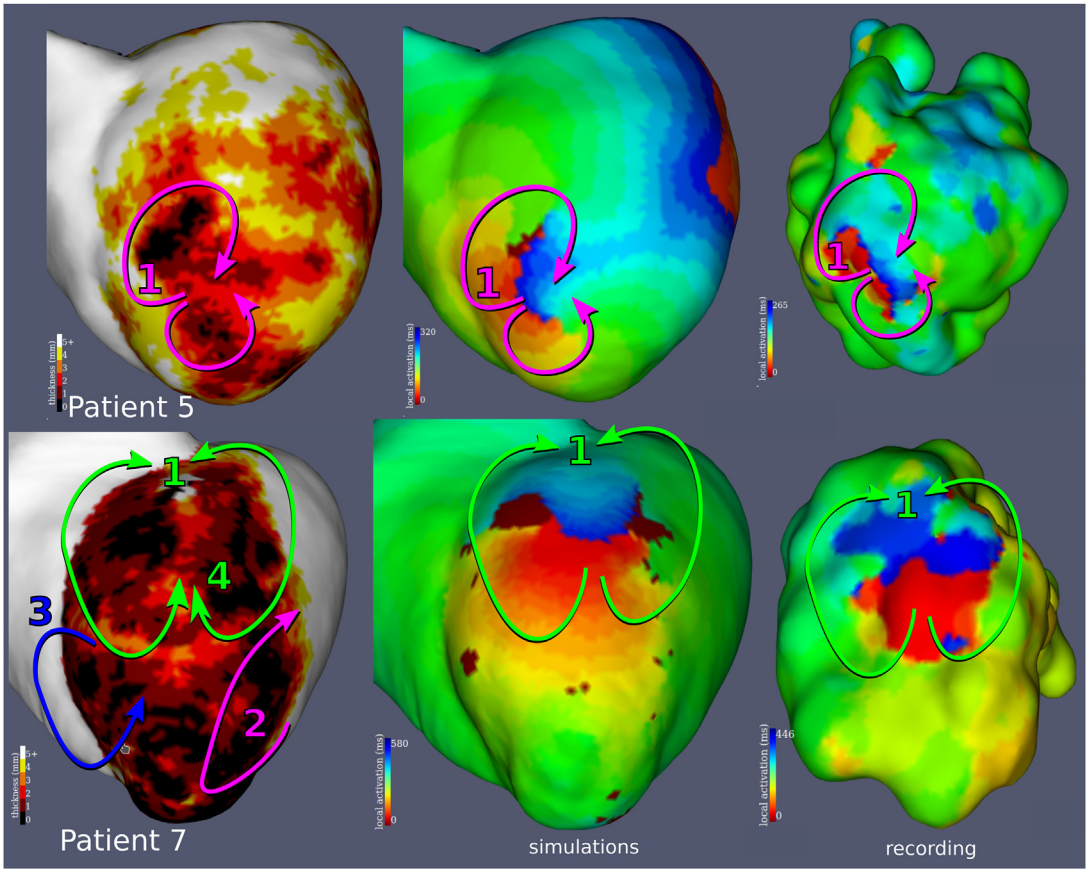

Simulated patterns in both cases successfully matched the ventricular tachycardia (VT) patterns in the electroanatomical map, revealing a typical figure-8 macro-re-entrant pattern with a central isthmus.

these CT-based models are less affected by ICD-induced artifacts than those of in vivo models built from CMR images.[6]

In addition, the associated 3D WT maps were generated using an automated segmentation method with a typical postprocessing segmentation time per case in the order of minutes on a consumer PC, which is advantageous for fast scar evaluations in the clinics. These WT maps were previously shown to correlate very well with scar and VT substrate location in clinical EAMs[11] and were found suitable for simulations.[18] The entire pipeline time frame (starting from acquiring the CT scans, to performing all the image processing steps, and to finally obtaining the simulation output) is only a matter of hours per case; thus, the clinical integration of our pipeline could be rapidly achieved in the foreseeable future.

SIGNIFICANCE OF HETEROGENEOUS ARI IN RELATION TO WT LEVELS. Second, the estimation of ARI (ie, the APD surrogate) from EP clinical data along with the fitting of associated restitution curves, led us to reveal a heterogeneity in ARI values as a function of different levels of myocardial WT (ie, lengthening of ARI in scarred zones where WT <3 mm, and shortening of ARI in zones with moderate WT of 3-5 mm). These APD heterogeneities may lead to a dispersion of repolarization within the suspected re-entry circuits, where tachyarrhythmia substrates are located. Our observations are in general agreement with experimental recent works that noted the existence of transient APD values during postinfarction healing, where surviving myocardial bundles within and adjacent to chronic scars may have either prolonged or shorter APDs compared to those in normal/remote tissue.[20,21] It has been shown that slow conducting areas within the suspected re-entry circuits are vulnerable to VT induction following rapid changes in pacing rates (such as those used in programmed S1-S2-S3 stimulations) but only if bundles of shorter APDs connect to bundles of longer APD, creating sharp transitions that generate directional blocks.[22] Thus, we suggest that the APD heterogeneity observed in our study has major arrhythmogenic implications, and, along with a slow conduction velocity in the suspected VT substrate, was likely an additional determinant factor in the inducibility of the 9 VT cases. However, we should emphasize that none of the experimental works have related the APD heterogeneity to different levels of WT in the infarcted territory, as defined by 3D tomographic imaging. In this respect, our study opens new possibilities to infer the alteration of physiological functions from structural imaging of scars.

Despite several encountered issues such as the noisiness of UEG signals, the imperfection of our ARI assessment algorithm and the uncertainty in the multimodal registration process, we believe that the substantially large amount of UEGs analyzed in this work makes our findings clinically relevant. To the best of our knowledge, this study is the first to exploit such relationships and to personalize biventricular heart models by integrating into predictive modeling not only estimated cardiovascular maps but also heterogeneous 3D ARI maps as key features associated to CT-defined WT levels.

IMPLEMENTATION AND PARAMETERIZATION OF THE PREDICTIVE MODEL. Concerning the selected computational approach, the monodomain formalism and Mitchell-Schaeffer model were adequate to model the transmembrane potential and VT inducibility; it has an intermediate complexity between highly detailed ionic models,[23] which need sophisticated solvers and supercomputers, and eikonal models, which lack the repolarization phase. In addition, in the meshless lattice Boltzmann method framework we employed, the spatial domain was discretized in a regular grid, which made it particularly suited to deal with voxels in CT image-based heart models; a fast graphics processing unit-based solver allowed us to complete the simulations from 100 pacing sites in 1-2 hours per case. If shown to be accurate, testing for VT inducibility virtually from multiple sites in a short amount of time would clearly have enormous incremental value as compared to the current standard of care that commonly tests 1-2 points during long and tedious invasive procedures. Moreover, multisite simulations can provide virtual insights into more potential VT paths and patterns than can be possibly revealed in the clinical study. Our selection aimed to cover all locations of potential ectopic beats that could trigger VTs in real life. Our simulations generated several distinct re-entry VT patterns, with at least 1 simulated pattern (or its mirror pattern) matching the clinically recorded VT pattern in 60% of the cases (ie, in 6 patients of the 9 who were clinically inducible). Importantly, among these simulated self-sustained VTs, the majority had a figure-8 morphology, a type of clinical VT that is predominantly present in scar-related VT cases and the target of ablation.

The results from this work also underline the importance of personalizing the model parameter that tunes APD from in vivo clinical data, unlike other computational works where the model parameters were customized using shorter/longer APD values taken either from literature on in vitro patch-clamp measurements[24] or from ex vivo epicardial optical

recordings.[25] In this respect, a strength of our current work is the novel approach to personalize the Mitchell-Schaeffer model by tuning the parameter that corresponds to APD as a function of different CT-defined WT levels, directly from clinical EAMs recorded in patients with scar-related VT. Moreover, in this study we used the exact same "transfer function" between CT images and EP features for all patients (excitability, APD, propagation speed); however, integrating other noninvasive sources of patient-specific data with clinical relevance (eg, medical history, ongoing medications, ECG features) may further personalize the model parameters of an individual heart and improve the model's output.

Finally, the grouping of simulated ECG waves led us to learn that different combinations of stimulation protocols and pacing sites could induce similar ECG wave morphologies during VT, as well as similar geometrical VT patterns (in terms of activation maps and isthmus). These VT morphologies and patterns were not random, but rather were driven by the topology of scar and VT circuits, as well as the location and size of critical channels (main or bystanders) relative to dense scars.

STUDY LIMITATIONS. Whereas this pilot study presents promising results, we acknowledge that it has some limitations. We used a small, retrospective cohort of patients in which we matched the simulated VT pattern to those recorded in the clinical study in 6 patients (of the 9 patients with documented inducible VT). Future work will address this by enlarging the database with more cases as well as using the pipeline for clinical prospective studies. Testing the model on larger cohorts of patients with scar-related VT will not only help estimate the arrhythmia risk, but also noninvasively find the ablation targets and help optimize the planning of radiofrequency ablation intervention.

Despite the high spatial resolution offered by CT imaging, it is possible that more complex propagation phenomena occur in some VT cases, such as those with intramural re-entry circuits or tortuous bystanders, which cannot all be accurately detected in CT images. Thus, we acknowledge that our structural models based on 3D CT-WT maps have limited capabilities of capturing some structural features and, consequently, predict accurately the VT paths associated with intramural isthmuses. Thus, besides the poor interpolation of recorded EAMs, this could have been a contributing factor to the mismatch between simulated and recorded VT patterns in all or some of those 3 patients (patients#4, 8, and 10, respectively). In this respect, the accuracy of fiber orientations could also play an important role. Therefore, using a human atlas of fibers[26] may lead to more accurate simulations of wave propagation and VT patterns compared to those we obtained using the ruled-based synthetic fibers. Lastly, several anatomical structures (eg, trabeculations, papillary muscles) that were included in our 3D CT-based models occluded part of the endocardial view, which is the reason we presented the qualitative comparison between simulated VT patterns in epicardial view vs the recorded VTs from endocardial EAMs.

Ideally, we would establish rules, like our APD rules, concerning the relationships among conduction velocity, CL, and wall thinning. However, computing velocities from clinically acquired data (inherently noisy, sparse, and with imperfect anatomical reconstruction) is extremely complicated, and that is why we settled for values found in the published reports instead.

Another simplification comes from the assumption that the model parameters for RVs matched those of healthy LVs, because we did not perform acquisition of intra-cardiac electrograms in RVs. Moreover, ICD lead artifacts were occasionally present; thus the RV wall could not be accurately segmented but instead was arbitrarily set to 5-mm thick by eroding the RV epicardial mask.

Moreover, another limitation related to our modeling approach, is the seemingly ad hoc compensation of the excitability parameters for physiologically thinner areas (apex and base). Although we are confident that this compensation is justified, we lack quantitative data to adjust it in a robust and objective way. As a potential solution, we plan to build an atlas of physiological LV thickness using the American Heart Association regions. Notably, our virtual inducibility protocols are more aggressive than those applied in the clinics where patient safety is a limiting factor; thus, the hyperexcitability must not be interpreted as an argument for the complete dismissal of our satisfying results.

Finally, most CLs computed from our simulated VTs slightly overestimated the recorded VTCL values. Primarily, VTCL directly depends on the wave speed (which varies on different segments of the re-entry circuit path, with the conduction velocity being reduced in the critical channels) and the perimeter of the scar. Thus, there are 2 possible reasons for the VTCL mismatch: 1) we used the 3D WT-based CV maps as in previous study,[18] instead of estimating the wave speed from EAMs; and 2) it is possible that the CT-derived WT maps slightly overestimated the

area/volume of dense scars (around which the VT wave rotates). However, this might be important only for cases with very small scars because those tend to generate faster and more dangerous VTCLs (associated with risk to degenerate into ventricular fibrillation), and these cases were not the focus of our current study.

FUNDING SUPPORT AND AUTHOR DISCLOSURES

This study received financial support from the French government as part of the "Investments of the Future" program managed by the National Research Agency (ANR-10-IAHU-04). The authors have reported that they have no relationships relevant to the contents of this paper to disclose.

ADDRESS FOR CORRESPONDENCE: Dr Nicolas Cedilnik, Epione Team, Inria, Université Côte d'Azur, 2004 route des Lucioles BP 93, 06 902 SOPHIA ANTIPOLIS Cedex, France. E-mail: nicolas.cedilnik@inria.fr.

PERSPECTIVES

COMPETENCY IN MEDICAL KNOWLEDGE: Chronic infarct scar is visible as ventricular wall thinning in CT imaging. The level of thinning is related to the degree of fibrosis and can be used to parameterize computational EP models. In silico induction protocols within this framework produce various macro-reentrant activation maps matching intracardiac recordings.

TRANSLATIONAL OUTLOOK: Our retrospective study suggests that VT ablation preprocedural planning could benefit from the use of computational simulations of induction protocols parameterized with CT imaging, to improve preidentification of re-entrant channels. Future efforts should be focused on confirming these findings in a prospective fashion.

REFERENCES

1. Zeppenfeld K, Tfelt-Hansen J, de Riva M, et al, ESC Scientific Document Group. 2022 ESC guidelines for the management of patients with ventricular arrhythmias and the prevention of sudden cardiac death. *Eur Heart J*. 2022;43(40):3997–4126.

2. Anderson RD, Lee G, Trivic I, et al. Focal ventricular tachycardias in structural heart disease: prevalence, characteristics, and clinical outcomes after catheter ablation. *J Am Coll Cardiol EP*. 2020;6(1):56–69.

3. Anter E. Limitations and pitfalls of substrate mapping for ventricular tachycardia. *J Am Coll Cardiol EP*. 2021;7(4):542–560.

4. Relan J, Chinchapatnam P, Sermesant M, et al. Coupled personalization of cardiac electrophysiology models for prediction of ischaemic ventricular tachycardia. *Interface Focus*. 2011;6;1(3):396–407.

5. Chen Z, Cabrera-Lozoya R, Relan J, et al. Biophysical modeling predicts ventricular tachycardia inducibility and circuit morphology: a combined clinical validation and computer modeling approach. *J Cardiovasc Electrophysiol*. 2016;27(7):851–860.

6. Prakosa A, Arevalo HJ, Deng D, et al. Personalized virtual-heart technology for guiding the ablation of infarct-related ventricular tachycardia. *Nat Biomed Eng*. 2018;2(10):732–740.

7. Balaban G, Halliday BP, Porter B, et al. Late-gadolinium enhancement interface area and electrophysiological simulations predict arrhythmic events in patients with nonischemic dilated cardiomyopathy. *J Am Coll Cardiol EP*. 2021;7(2):238–249.

8. Mahida S, Sacher F, Dubois R, et al. Cardiac imaging in patients with ventricular tachycardia. *Circulation*. 2017;19;136(25):2491–2507.

9. Perez-David E, Arenal A, Rubio-Guivernau JL, et al. Noninvasive identification of ventricular tachycardia-related conducting channels using contrast-enhanced MRI in patients with chronic myocardial infarction: comparison of signal intensity scar mapping and endocardial voltage mapping. *J Am Coll Cardiol*. 2011;57(2):184–194.

10. Lozoya RC, Berte B, Cochet H, et al. Model-based feature augmentation for cardiac ablation target learning from images. *IEEE Trans Biomed Eng*. 2019;66(1):30–40.

11. Takigawa M, Duchateau J, Sacher F, et al. Are wall thickness channels defined by computed tomography predictive of isthmuses of post-infarction ventricular tachycardia? *Heart Rhythm*. 2019;16(11):1661–1668.

12. Ghannam M, Cochet H, Jais P, et al. Correlation between computer tomography-derived scar topography and critical ablation sites in post-infarction ventricular tachycardia. *J Cardiovasc Electrophysiol*. 2018;29(3):438–445.

13. Wyatt RF, Burgess MJ, Evans AK, et al. Estimation of ventricular transmembrane action potential durations and repolarization times from unipolar electrograms. *Am J Cardiol*. 1981;47:488.

14. Orini M, Srinivasan N, Graham AJ, et al. Further evidence on how to measure local repolarization time using intracardiac unipolar electrograms in the intact human heart. *Circ Arrhythm Electrophysiol*. 2019;12(11):e007733.

15. Djabella K, Landau M, Sorine M. *A two-variable model of cardiac action potential with controlled pacemaker activity and ionic current interpretation. In: 2007 46th IEEE Conference on Decision and Control*. IEEE; 2007:5186–5191.

16. Mitchell CC, Schaeffer DG. A two-current model for the dynamics of cardiac membrane. *Bull Math Biol*. 2003;65(5):767–793.

17. Rapaka S, Mansi T, Georgescu B, et al. LBM-EP: lattice-Boltzmann method for fast cardiac electrophysiology simulation from 3D images. *Med Image Comput Comput Assist Interv*. 2012;15(Pt 2):33–40.

18. Cedilnik N, Duchateau J, Dubois R, et al. Fast personalized electrophysiological models from computed tomography images for ventricular tachycardia ablation planning. *Europace*. 2018;20(suppl 3):iii94–iii101.

19. Streeter DD, Spotnitz HM, Patel DP, et al. Fiber orientation in the canine left ventricle during diastole and systole. *Circ Res*. 1969;24(3):339–347.

20. Srinivasan NT, Orini M, Providencia R, et al. Prolonged action potential duration and dynamic transmural action potential duration heterogeneity underlie vulnerability to ventricular tachycardia in patients undergoing ventricular tachycardia ablation. *Europace*. 2019;21(4):616–625.

21. Denisko D, Oduneye S, Krahn P, et al. Analysis of activation-recovery intervals from intracardiac electrograms in a pre-clinical chronic model of myocardial infarction. *Lect Notes Comput Sci*. 2017;10263:280–288.

22. Kelemen K, Greener ID, Wan X, et al. Heterogeneous repolarization creates ventricular

tachycardia circuits in healed myocardial infarction scar. *Nat Commun*. 2022;13(1):830.

23. Luo CH, Rudy Y. A model of the ventricular cardiac action potential: depolarization, repolarization, and their infarction. *Circ Res*. 1991;68(6):1501-1526.

24. Arevalo HJ, Vadakkumpadan F, Guallar E, et al. Arrhythmia risk stratification of patients after myocardial infarction using personalized heart models. *Nat Commun*. 2016;7(1):11437.

25. Pop M, Sermesant M, Liu G, et al. Construction of 3D MR image-based computer models of pathologic hearts, augmented with histology and optical fluorescence imaging to characterize action potential propagation. *Med Image Anal*. 2012;16(2):505-523.

26. Lombaert H, Peyrat JM, Croisille P, et al. Human atlas of the cardiac fiber architecture: study on a healthy population. *IEEE Trans Med Imaging*. 2012;31(7):1436-1447.

KEY WORDS action potential duration, imaging, ischemic scar, simulation, ventricular tachycardia

APPENDIX For an expanded Methods section, and supplemental tables and a figure, please see the online version of this paper.